Tellus (2004), 56B, 285–293
Printed in UK. All rights reserved

TELLUS

Observations of the impact of cloud processing on aerosol light-scattering efficiency

By DEAN A. HEGG[1]*, DAVID S. COVERT[2], HAFLIDI JONSSON[3], DJAMAL KHELIF[4] and CARL A. FRIEHE[5], [1]*Department of Atmospheric Sciences, Box 351640, University of Washington, Seattle, WA 98155, USA;* [2]*Department of Atmospheric Sciences, Box 351640, University of Washington, Seattle, WA 98155, USA;* [3]*CIRPAS, Naval Postgraduate School, PO Box 550, Marina, CA 93933, USA;* [4]*Department of Mechanical and Aerospace Engineering, MS 3975, University of California at Irvine, Irvine, CA 92697-3975, USA;* [5]*Department of Mechanical and Aerospace Engineering, MS 3975, University of California at Irvine, Irvine, CA 92697-3975, USA*

(Manuscript received 16 July 2003; in final form 10 December 2003)

ABSTRACT

Airborne data are presented on the impact of cloud processing on the aerosol mass light-scattering efficiency. The measurements, on marine stratocumulus, suggest that cloud processing significantly enhanced the mass light-scattering efficiency in three of the five cases analysed. Enhancements were of the order of 10% for air detraining from the cloud deck relative to non-detraining air. A diagnostic modelling analysis suggested that the observed enhancements were consistent with the previously proposed explanation of in-cloud sulfate production in the particle size range for efficient light scattering.

1. Introduction

The efficiency with which anthropogenic aerosols scatter light, i.e. the total light scattering per unit mass of aerosol, is an important parameter in the estimation of the direct radiative forcing of climate by anthropogenic aerosols (e.g. Charlson et al., 1992; IPCC, 2001). Much of the anthropogenic aerosol in the Northern Hemisphere (the locus of the preponderance of anthropogenic radiative forcing by aerosols) is sulfate, derived largely from emissions of gaseous SO_2 followed by *in situ* oxidation in the atmosphere (IPCC, 2001). This oxidation takes place either in the gas phase or in the aqueous phase of clouds. Lelieveld and Heintzenberg (1992) have made the important prediction that, due to the differing aerosol size of the mass created by these processes, its scattering efficiency will also vary over the range from $\sim$2 to 8 m^2 g^{-1}, with the in-cloud production yielding the higher efficiency. However, a number of factors render the significance of the dichotomy between cloud and clear-air derived scattering efficiencies less straightforward than might at first appear. One straightforward, practical consideration is simply the relative contribution of the oxidation pathways. While there is consensus that the aqueous pathway dominates globally, there is substantial temporal and spatial variability in their relative importance (cf. Hegg, 1985; Lelieveld, 1991; Langner and Rodhe, 1991). Hence, for any particular locale, climatology will strongly modulate the effect. In the same vein, Lelieveld and Heintzenberg themselves point out that the magnitude of the dichotomy in scattering efficiency diminishes with the amount of sulfate produced per unit volume of air. One might therefore expect variability in scattering efficiency as a function of the SO_2 source distribution as well, with the most marked contrast in efficiencies in cleaner air, such as marine venues. Finally, and more fundamentally, more detailed assessments of the aqueous conversion pathway have shown that the magnitude of the change in scattering efficiency of cloud-processed aerosol, and thus of the pathway dichotomy, will be a strong function of the initial aerosol size distribution and, in particular, the presence of a coarse as well as an accumulation mode in the particle size distribution (Hegg et al., 1992; Yuen et al., 1994).

Given the potentially important dependence of the aerosol light-scattering efficiency on the aerosol production pathway, it is rather surprising that more effort has not been devoted to its experimental investigation in the field. There have indeed been several studies over the years which have measured aerosol light scattering near or even in clouds (e.g. ten Brink et al., 1987; Yuskiewicz et al., 1998) without documenting any significant effect of cloud processing on the light-scattering efficiency but only one which directly confronted the issue and was in fact designed to do so. This study, that of Yuskiewicz et al. (1999), examined the impact of passage through an orographic wave-cloud on the aerosol size distribution, and the aerosol

*Corresponding author.
e-mail: deanhegg@atmos.washington.edu

light-scattering efficiency calculated from Mie theory based on the pre and post-cloud size distributions.

Yuskiewicz et al. (1999) found changes in the aerosol size distribution associated with in cloud sulfate production which enhanced the calculated downwind aerosol scattering efficiency compared with that estimated for the upwind samples. Extensive comparison with the predictions of both Yuen et al. (1994) and Lelieveld and Heintzenberg (1992) were also undertaken, with some consistency established between the earlier predictions and the observations. However, there are two related issues that somewhat circumscribe the decisiveness of the presented results. First, the scattering efficiency was not directly measured (aerosol light scattering was not measured) but rather predicted from the Mie scattering calculations performed on the measured size distributions. Size distribution measurements have large uncertainties (commonly of the order of ±25% for particle size alone) for any given size of particle and there is additional uncertainty associated with the choice of the refractive index to use in the calculations. Given the strong functional dependence of scattering coefficient on particle size (the dependence is third order for the size range measured by Yuskiewicz et al. 1999) the synthetic scattering efficiencies derived in the study have quite large uncertainties. For example, for a third-order size dependence, a 25% uncertainty in size would by itself produce a 75% uncertainty in scattering coefficient. Second, as Yuskiewicz et al. (1999) themselves point out, the size distribution measurements truncate at 0.8 μm diameter, thus precluding the determination of any coarse mode present (or any supermicron component at all). The impact of the coarse mode on the size distribution of sulfate produced in cloud renders any scattering efficiencies calculated without inclusion of this mode suspect (cf. Hegg et al., 1992). For these reasons, further measurements of the impact of cloud processing on aerosol light-scattering efficiency seemed in order and led to the experiment discussed below.

2. Methodology

The data reported and analysed here were gathered during the CARMA-I study (Cloud-Aerosol Research in the Marina Atmosphere) conducted off the mid-California coast during August and early September of 2002. The location and timing of the experiment were selected to maximize the occurrence and duration of marine stratocumulus within easy reach of the aircraft base of operations at Marina, CA (on Monterey Bay). The summer stratocumulus deck in this locale is quite stable, persisting, with occasional breaks, for weeks at a time. While the cloud deck is typically only a few hundred metres thick, vertical velocities are also modest (from ~0.1 to 2 m s^{-1}) and yield substantial in-cloud residence time for entrained air parcels—and thus sufficient time for significant aqueous sulfate production. Additionally, the deck is reasonably well-understood dynamically and thus susceptible to modelling.

The aircraft instrumentation platform used in this study was the CIRPAS Twin Otter research aircraft. This aircraft has been described, in part, in a number of previous studies (e.g. Gao et al., 2003). The instruments relevant to the current analysis are shown in Table 1. The key parameters are the dry aerosol light-scattering coefficient at 550 nm, measured by the nephelometer with a pre-heater to reduce relative humidity (RH) to ~30% or less, and the aerosol dry volume, measured by integration of the passive cavity aerosol spectrometer probe (PCASP-100X) size distribution operating with the de-icing heaters on to reduce the measurement RH to ~40% or less. Several issues such as calibration, signal processing and time response arise with respect to the utilization of these instruments.

The nephelometer was calibrated with particle-free air and CO_2 as described in, for example, Anderson and Ogren (1998). The instrument was operated with no real-time electronic signal averaging to enhance time response, and the output

Table 1. Instruments aboard the Twin Otter research aircraft during CARMA-I which were utilized in the current study

Instrument	Parameter measured	Manufacturer	Measurement uncertainty
Nephelometer	Aerosol light-scattering coefficient at 3 wavelengths	TSI Inc. model 3563	±3 Mm^{-1}
Optical particle counter	Aerosol size distribution from 0.1 to 3.2 μm diameter	PMS/DMT model PCASP-100X	Variable, ~ ± 25% in size (±10% for constant index of refraction), $\sqrt{N}$ in concentration
Optical particle counter	Cloud drop size distribution from 2 to 40 μm diameter	PMS/DMT model FSSP-100	Variable, ~ ± 25% in size, $\sqrt{N}$ in concentration
Hotwire	Cloud liquid water content	DMT Model CAPS	± 0.1 g m^{-3}
Capacitance sensor	RH/dewpoint	Vaisala model Humicap FI	±3%
Chilled mirror	Dewpoint	EG&G	±1 °C
Radome pressure array	3-D winds	UCI/CIRPAS (Setra Transducers)	± 0.2 m s^{-1}
RTD	Temperature	Rosemount model 102E4AL	±0.2 °C
UV absorption photometer, Lyman-alpha	Absolute humidity		± 0.05 g m^{-3}
Filter cassettes	Sulfate concentration	Gelman/in-house	Sample dependent

signal was corrected as suggested in Anderson and Ogren (1998). The sample flow rate utilized was 40 l min^{-1}, once again to enhance time response. At this flow, significant impaction of particles within the instrument can be expected for particles above 5 μm diameter. The nephelometer was located within the aircraft fuselage and sampled through a shrouded aerosol inlet consisting of two serial diffuser cones to decelerate the flow. The transmission efficiency of the inlet was determined by intercomparison of cross-calibrated forward scattering spectrometer probe (FSSP-100) spectrometers, one located on the aircraft wing and one within the fuselage sampling just downstream of the nephelometer. Comparison of the in-flight particle spectra from the FSSPs revealed an inlet 50% cut point of 8 μm diameter and a passing efficiency at 3 μm (the upper limit of the PCASP-100X) of 90%. Finally, the overall time response of the inlet–nephelometer system was tested on the ground. A blower was attached to the main sample line exhaust to pull air through the system at the 7 m s^{-1} flow rate measured during flight. A step function aerosol source was introduced at the shroud inlet and the delay time until detection by the nephelometer was measured. An average delay time of 2 s was established.

The PCASP-100X was used for aerosol sizing in part because it covers the range of particle sizes that contribute appreciably to light scattering under most conditions in the atmosphere and in part because it has been extensively used and has well-known response characteristics. We calibrated it in a manner similar to that reported by Liu et al. (1992) using NaCl, polystyrene latex (PSL) and di-octyl sebacate (DOS) spheres (indices of refraction ranging from 1.33 to 1.58). The sizing uncertainty for a single index of refraction was $\pm$10% while differing indices of refraction expanded the uncertainty to $\pm$25%. This is the basis for the numbers given in Table 1. We note that for our sampling scenario, in which the refractive index changes negligibly between samples we compare, $\pm$10% is a reasonable estimate of sizing uncertainty. With respect to the comparability of PCASP and nephelometer data, although the instruments have slightly different effective upper size limits, the measured size distributions during the study suggest a negligible aerosol volume in the 3–5 μm window between these upper limits ($\sim$2% of the total volume).

The ratio of the light-scattering coefficient measured by the nephelometer to the PCASP aerosol volume is the light scattering per unit aerosol volume. This is converted to the aerosol mass scattering efficiency using an assumed dry density of 1.8 g cm^{-3}, consistent with other studies (e.g. Yuskiewicz et al., 1999). Filtration-based aerosol composition measurements were also undertaken in this study using filters and procedures described in Gao et al. (2003). While the only chemical composition data directly utilized in this study were sulfate concentrations, the overall aerosol composition was dominated by sea salt and sulfate, with lesser fractions from organics and nitrates. The density of this mix is consistent with the value of 1.8 g cm^{-3}.

The wind/turbulence instrumentation system on the aircraft was similar to that used on other research aircraft (cf. Khelif et al., 1999) and consisted mainly of fast-response sensors to measure the 3-D wind vector, temperature and humidity. A five-hole radome pressure port system (Brown and Friehe, 1983) was used for measurement of the mean and fluctuating airspeed vector (magnitude and attack and slip angles). The aircraft motion and altitude angles required for calculation of earth-based winds are measured at 10 Hz using a modern integrated GPS/IN unit. Means and fluctuations of temperature were obtained from redundant Rosemount 102E4AL probes and UCI-modified Rosemount probes (Friehe and Khelif, 1992). Humidity fluctuations were obtained from two Lyman-alpha humidiometers (Buck, 1976), which were calibrated using the method described in Friehe et al. (1986). The data were all sampled and stored at 40 Hz.

The basic flight plan for CARMA-I involved 15–20 min flight legs at various altitudes either parallel to or transverse to the mean wind (some legs were also flown along sea surface temperature (SST) or aerosol gradients). In general, a leg would be flown close to the sea surface, one just below cloud base, one in-cloud and one just above the cloud top. Vertical profiles through the marine boundary layer (MBL) were also obtained in the operations area on each flight. For this study, the key leg was that at cloud top, during which data were obtained on aerosol detraining from the cloud layer. Detailed discussion of the approach adopted to discern the detrainment is deferred to the discussion of the results. The cloud-base flight leg, when coupled with the spiral profiles, provided data to initialize modelling work, while the in-cloud data were utilized as a check on the model predictions.

3. Results and discussion

3.1. Database

The CARMA-I field experiment had several objectives in addition to the one at issue in this study. Hence, not every flight was optimized to examine the impact of cloud processing on the aerosol light-scattering efficiency. Of the 13 flights executed during CARMA-I, nine had significant flight legs above the stratocumulus cloud top. However, in two cases the flight level was too high above the cloud top to render differentiation of entraining and detraining air feasible. Two other cases revealed very significant horizontal temperature gradients, which obscured differences in temperature and RH due to vertical motions. Consequently, five flights form the data base for the analysis presented here. Table 2 summarizes the general aerosol characteristics for these five flights.

3.2. Data analysis

The most straightforward methodology for assessing a possible enhancement in aerosol light-scattering efficiency due to cloud

Table 2. Research flights and selected results bearing on aerosol light-scattering efficiency. Note that σ_{SP} is the aerosol light-scattering coefficient while the various subscripted αs refer to the light-scattering efficiency at cloud base (CB), cloud-top detraining (CTD) and cloud top non-detraining (CTND). Also note that values given for the efficiencies are means and standard errors of the means over the various flight legs (see text)

Flight date	Sample time	Location	Altitude	σ_{SP} (Mm^{-1})	α_{CB} ($m^2\ g^{-1}$)	α_{CTD}($m^2\ g^{-1}$)	α_{CTND} ($m^2\ g^{-1}$)
8/23	21:17–21:51	36.2 – 36.5N, 122.47–122.95W	840 m	165	4.7 ± 0.03	5.6 ± 0.05	5.1 ± 0.06
8/24	21:32–21:35	36.9–37.0N, 122.8–123.1W	561	79	4.3 ± 0.04	6.3 ± 0.5	5.1 ± 0.1
8/28	22:46–22:52	36.9–37.0N, 123.4–123.8W	524	25	4.3 ± 0.08	4.2 ± 0.15	4.2 ± 0.06
9/01	20:55–21:21	35.6–36.1N, 123.1–123.4W	249	48	4.1 ± 0.08	4.7 ± 0.1	4.1 ± 0.08
9/03	18:33–18:40	36.1–36.1N, 122.4–122.6W	450	52	4.2 ± 0.06	4.5 ± 0.13	4.4 ± 0.09

processing, at least for the essentially horizontally homogeneous scenarios of this study, would be to examine vertical profiles of scattering efficiency through the cloud deck and look for positive anomalies near the cloud edges. Figure 1 shows several examples of such profiles for flights during CARMA-I. It can be seen that there is indeed a positive anomaly at cloud top (note that the very low scattering efficiencies just below the inversions help delineate the location of the cloud decks) for the cases of 23 and 24 August (8/23 and 8/24), while 28 August (8/28) shows no such structure. The peaks in scattering efficiency are quite restricted in altitude, as might be expected from a detraining scalar mixing into ambient air, with a peak thickness of ~25 m. Averaging the scattering efficiency over the peak thickness, the cloud-top peak on 8/23 had a value of $7.2 \pm 0.1\ m^2\ g^{-1}$ in comparison to a cloud base 25 m average of $5.4 \pm 0.04\ m^2\ g^{-1}$. Similarly, for the case of 8/24, the higher altitude peak above cloud top had a value of $7.7 \pm 0.1\ m^2\ g^{-1}$, the lower cloud-top peak a value of 5.1 ± 0.1 and the cloud-base mean a value of $4.9 \pm 0.1\ m^2\ g^{-1}$. In contrast, for the case of 8/28, the cloud-top peak has a value of $4.8 \pm 0.1\ m^2\ g^{-1}$ compared with a cloud-base value of 5.2 ± 0.1. Hence, for the last case, cloud processing would appear to have a negligible impact. Furthermore, for the case of 8/24, there is some ambiguity as to which cloud-top peak to utilize and thus ambiguity as to whether or not a significant enhancement in scattering efficiency has occurred. The two remaining flights in Table 2 do show scattering anomalies at cloud top but they are equally indefinite. It would clearly be preferable to have longer sampling times at each altitude to enable signal averaging and consequent noise reduction. While this is not feasible during a rapid spiral ascent or descent, it could be done during a cloud-top level traverse if one could differentiate between air detraining from the cloud below and air descending into the cloud or essentially stationary at the flight level.

The structure and dynamics of marine stratocumulus, such as that sampled in this study, are fairly well known, both observationally and theoretically (cf. Martin et al., 1995; Kogan et al., 1994; Stull, 1988). The turbulent mixing process which is a major driving force in maintaining the stratocumulus results in a cloud consisting of a collection of rising and falling air parcels, the rising parcels associated with detraining of air at cloud top. The spatial scale of these parcels or, equivalently, the associated turbulent eddies, is highly variable and generally described best by a broad distribution function. However, the most effective transport through the cloud layer will be at eddy scales comparable to the vertical thickness of the cloud—100–300 m for the cases analysed here. Given the typical airspeed of the Twin Otter, 50–55 m s^{-1}, instruments with time responses of less than 2–3 s should be capable of resolving these eddies and thus differentiating air parcels moving up (detraining) through cloud from those originating at or above cloud top. The two instruments from which the aerosol scattering efficiency is derived, the nephelometer ($\tau \sim 2$ s) and the PCASP-100X ($\tau = 1$ s) can certainly do this. Hence, a viable approach to differentiating the scattering efficiency of recently cloud-processed air from everything else would simply be to average over the detraining eddies. This is essentially equivalent to the well-known technique of averaging over parcels of different sorts to resolve components of the total kinetic energy (TKE) budget (e.g. Moenig, 1987) but still necessitates a choice of parameter to delineate the detraining eddies. Such an averaging procedure has the added advantage of minimizing the impact of measurement uncertainties. Both measurement and sampling uncertainties can be characterized by the standard error of the mean values and will be relatively small for the large number of sample points (10^2–10^3) contributing to the mean values. Vertical momentum (e.g. vertical velocity) is an obvious choice for the tracer variable, but since pressure forces contribute to its transport, the resulting correlation with scalars such as aerosol concentration and scattering coefficient is smeared out. Scalars such as temperature and humidity are more appropriate since pressure does not directly affect their transport (cf. Pasquill, 1974). Fortunately, the MBL thermodynamic structure in the cases examined here provide a clear-cut opportunity to use such tracers for detection of recently cloud-processed air.

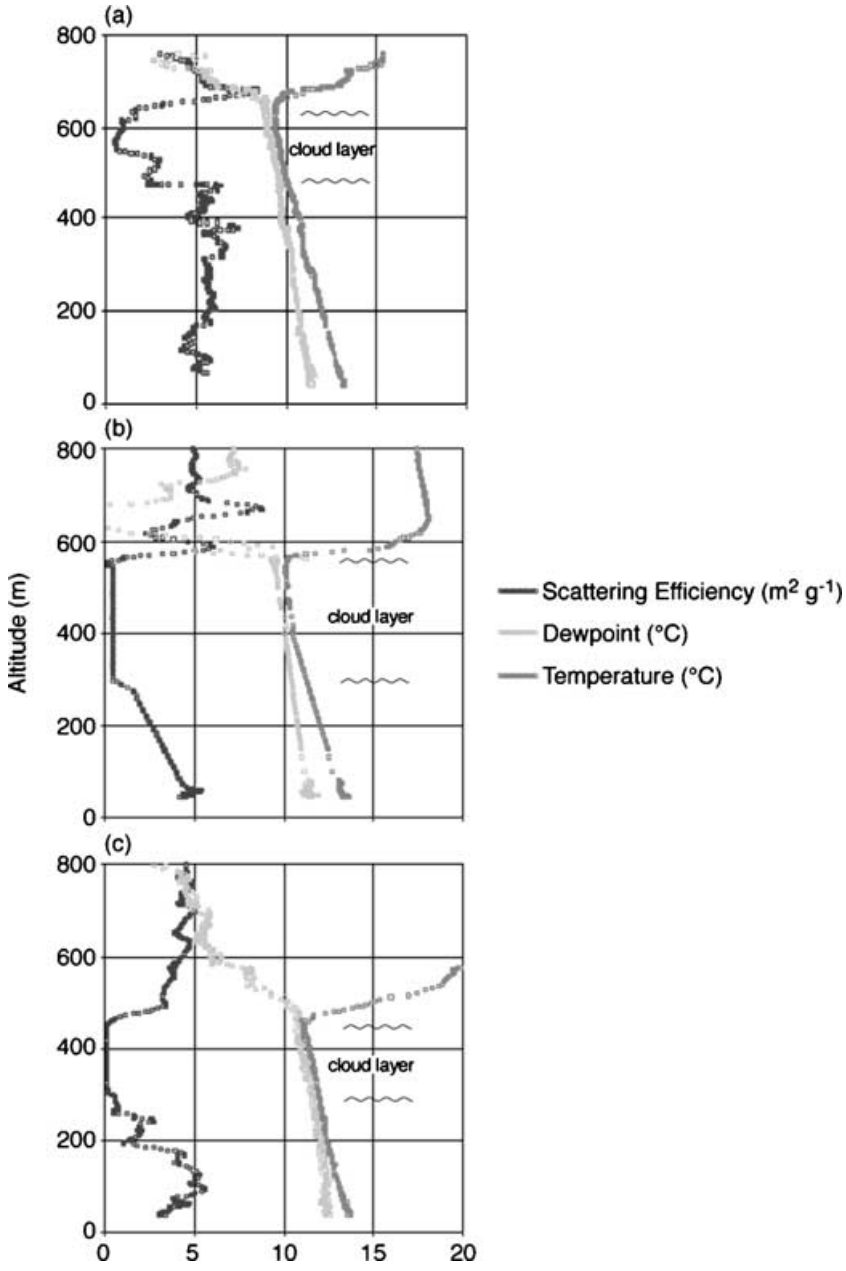

Fig 1. Vertical profiles of the aerosol light-scattering efficiency together with soundings of ambient temperature and dew point on three CARMA-I flights, 23 August (a), 24 August (b) and 28 August (c) 2002. The depressed efficiency just below the inversion base is due to the presence of cloud.

Shown in Fig. 1, in addition to the scattering efficiency profiles, are temperature and dew point soundings for each of the cases presented. Typically five such soundings were taken on each flight, all showing the same general MBL structure (i.e. horizontal homogeneity was confirmed). The sampling flight level in all cases was just above the inversion base, i.e. at cloud top. Examining the first case, 8/23, it is quite clear that air sampled at cloud top with temperatures less than 12 °C or dew points greater than 9 °C, or, equivalently, absolute humidities greater than $\sim$7 g m^{-3}, must necessarily have come up through the cloud from below. As might be expected, all of the cloud-topped MBL cases examined here show similar profiles though, of course, the temperature and water vapour mixing ratio criteria needed to clearly differentiate cloud-processed air from other air differ from case to case. With the vertical structure illustrated in Fig. 1 in mind, we next examine the time series for temperature and water vapour in a cloud-top run.

In Fig. 2, 25 s time series (of 40 Hz data) for water vapour mixing ratio and air temperature are shown for the cloud-top run associated with the vertical profile of Fig. 1a. Three detraining parcels or eddies are evident, together with two areas of vertically quiescent or possibly downward-moving air. Each of these is on the order of 3 to 5 s (or 150 to 250 m) wide, in accord with our hypothesized effective eddy scale, and shows the

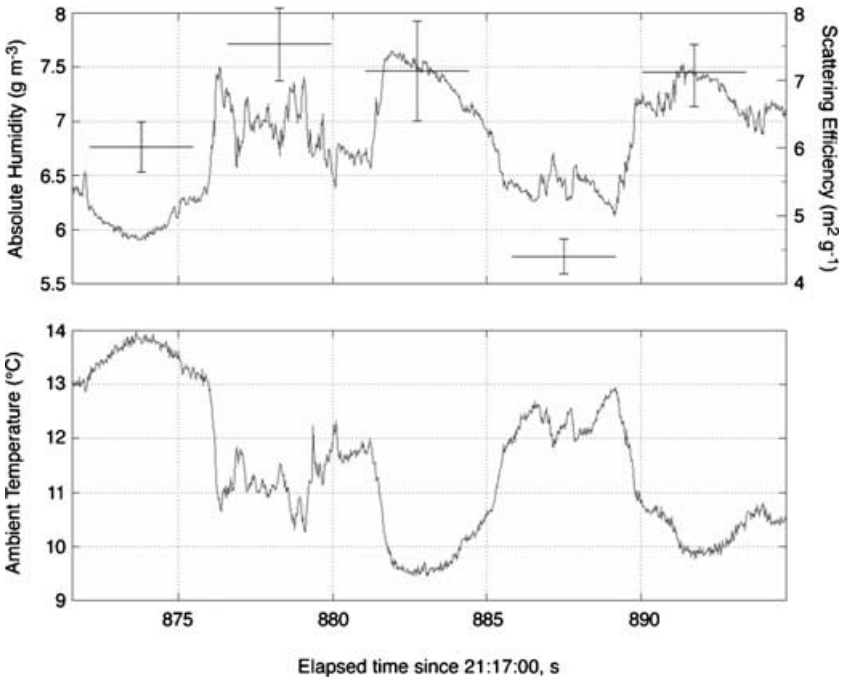

Fig 2. Time series of absolute humidity (Lyman-alpha hygrometer), temperature (Rosemount platinum wire) and aerosol mass light-scattering efficiency for a segment of the cloud-top run on 23 August. The data rate is 40 Hz for the humidity and temperature data. The scattering efficiencies are 5 s averages of 1 Hz data.

expected strong negative correlation between temperature and water vapour mixing ratio. For each of the five distinct regions, mean values (5 s) of 1 Hz data on the aerosol mass scattering efficiency have been calculated and superposed on the absolute humidity trace. There is clearly a strong correlation between areas of detrainment and high scattering efficiency. Given these results, average values for aerosol light-scattering efficiency have been calculated for each cloud-top run, stratified to separate detraining from non-detraining air. As a reference, the mean light-scattering efficiency for each associated cloud-base run has also been calculated. These results are shown in Table 2.

From Table 2, it can be seen that in four of five cases the scattering efficiency for the detraining air is larger than that of the non-detraining air samples. In three of the five cases it is significantly larger and in no case is it smaller. Similarly, in four of five cases the cloud-base scattering efficiency is smaller than that of the aerosol detraining at cloud top and in no case is it significantly larger. The mean value for the cloud-enhanced scattering efficiency is 5.1 ± 0.9 m^2 g^{-1}, in remarkable agreement with the value of 5.0 ± 0.3 m^2 g^{-1} reported by Yuskiewicz et al. (1999), though clearly this is in part fortuitous. On the other hand, the fractional enhancement in scattering efficiency of the detrained air compared with the residual is a modest 10%, on average. This is in contrast to the enhancement of roughly a factor of 2 predicted by Lelieveld and Heintzenberg (1992) for similar in-cloud sulfate production. However, as noted previously, the magnitude of any enhancement is strongly dependent on the initial size distribution prior to cloud processing. The size distribution selected by Lelieveld and Heintzenberg (1992) is quite different from those measured during CARMA-I, having a very modest coarse mode and substantially smaller accumulation modal radius. Furthermore, there is an important conceptual issue here. Lelieveld and Heintzenberg (1992) compare their cloud-processed scattering efficiency with one derived solely from gas-phase sulfate production. In contrast, the enhancements observed here are between a just-detrained air parcel and air that also has a component that was probably also cloud processed, just not quite so recently.

The proximate cause of the enhanced light-scattering efficiency due to cloud processing is a shift of the size distribution toward the effective light-scattering size range, essentially the first Mie resonance peak. While the observed differences in size distribution are slight between the detrained air and the residual air, they are consistent with this prediction. This can be seen in Fig. 3, in which the mean detrained spectrum at cloud top does shift more into the size range of effective scattering compared with the non-detrained average spectrum.

3.3. Modelling the observed effect

As a further check on the viability of the rationalization offered here for the observed enhancement in aerosol light-scattering efficiency, model calculations are performed for the three cases shown in Table 2 in which significantly enhanced efficiencies were measured in detraining air. The model which will be utilized is the explicit microphysical parcel model used by Yuen et al. (1994). The model will be initialized on the mean measured aerosol size distribution at cloud base, the measured cloud-base thermodynamic data, and the updraft velocity measured in the ascending eddies. The initial aerosol size distributions used for each of the three cases examined are shown in Fig. 4. Since no

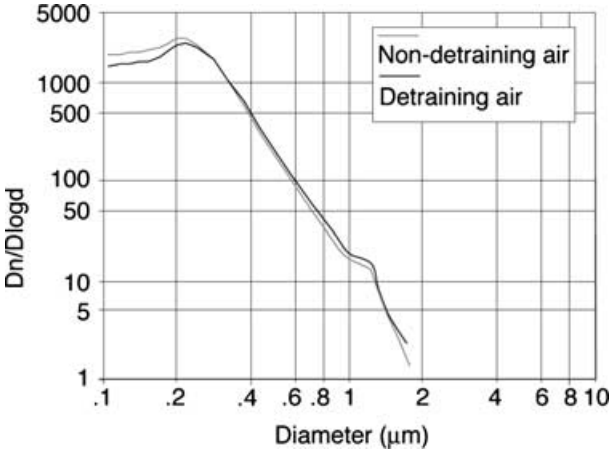

Fig 3. Aerosol number size distributions averaged over detraining and non-detraining air at cloud top obtained on 23 August. The abscissa is geometric diameter.

measurements of SO_2, O_3 or H_2O_2 are available to initialize the model, estimates from past studies must be utilized. For O_3 this is not a severe problem since it varies little at this time of year and at this locale—and there is always excess O_3. For SO_2, we shall use past measurements by Bates et al. (1992) in roughly the same area. For H_2O_2, we will use data from O'Sullivan et al. (1999) and Heikes et al. (1996) in this same area. The concentrations of SO_2 and H_2O_2 will be varied to yield sulfate concentrations from in-cloud oxidation similar to those observed from the filter sampling. Sensitivity studies with the model have shown that sulfate production is essentially linear in initial SO_2 concentration for the other initial conditions utilized here. Such production is insensitive to H_2O_2 concentration at or above 1 ppbv (part per billion by volume).The gas-phase concentrations used were: $H_2O_2 = 1$ ppbv for all flights, $O_3 = 30$ ppbv for all flights, $SO_2 = 300$ pptv (parts per trillion by volume) for 8/23 and 1 September (9/01) but 200 pptv for 8/24. While these are reasonable estimates, because of the lack of directly measured gas concentrations, the calculations should not be considered prognostic, or definitive. Our goal is simply to determine if observed aerosol size distributions, when processed by clouds with observed microphysics and accumulating extra mass consistent with observed sulfate production, experience an enhancement in the aerosol light-scattering efficiency similar to that observed. Essentially, it is an assessment as to whether or not the observed enhancement in efficiency is consistent with the proposed mechanism.

Results for the model runs, and a comparison with observations, for the three cases that showed significant enhancements of light-scattering efficiency, are shown in Table 3. With respect to the cloud properties, the model calculations capture the liquid water content (LWC) well but systematically underpredict the cloud drop number concentration (CDNC). This is likely to be simply due to transient high vertical velocities in cloud not well

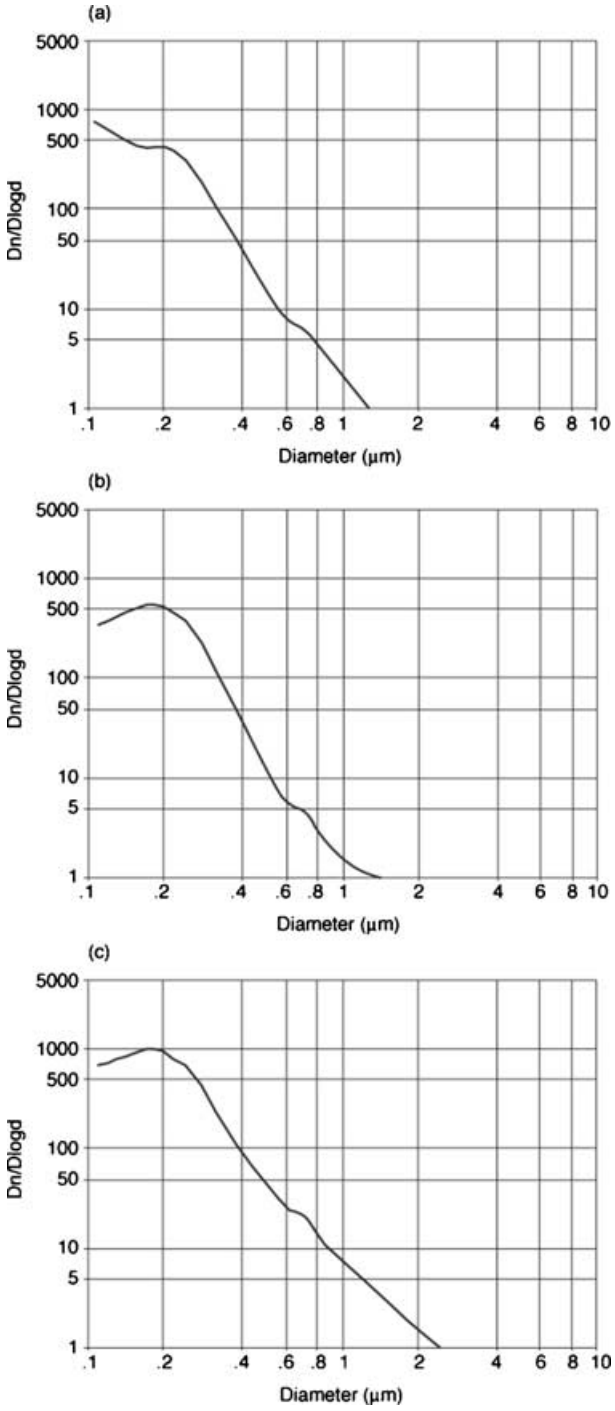

Fig 4. Aerosol size distributions used to initialize the MLM model: (a) distribution for 23 August, (b) for 24 August and (c) for 1 September.

represented by the mean values used to initialize the model. For the first two flights shown, the model predicted sulfate production is also in reasonable agreement with the observations. However, plausible concentrations of H_2O_2 and SO_2 cannot reproduce the observed sulfate production on 09/01. It is of course possible that anomalously high concentrations were present, though there is

Table 3. Comparison of modelled enhancements in the aerosol light-scattering efficiency with observed enhancements. Also shown are comparisons of modelled with observed cloud and aerosol parameters. Comparisons are given as: observed/modelled

Flight date	Liquid water content (g m^{-3})	CDNC (cm^{-3})	Sulfate produced ($\mu g\ m^{-3}$)	Change in scattering efficiency (%)
08/23	0.55/0.53	250/201	0.54/0.31	10/2
08/24	0.60/0.57	250/182	0.06/0.07	12/1
09/01	0.40/0.30	450/352	0.85/0.1	7/2

nothing present in the available data to support this. The critical comparison is, of course, that between modelled and observed aerosol light-scattering efficiencies. The model systematically underpredicts this parameter. Reasons for a discrepancy are not hard to find. For example, the precise size distribution of the sulfate produced in cloud is not simply a function of the initial size distribution but of such variables as the distribution of droplet pH over size, variables that are rarely if ever measured in any field project. Similarly, in-cloud collection processes may well have altered the size distribution of the sulfate produced in the cloud. Nevertheless, the key point is that the model does predict an enhancement in the light-scattering efficiency, in accord with observations.

4. Conclusions

Field observations are reported which suggest enhancement of the aerosol light-scattering efficiency due to cloud processing, in accord with the hypothesis of Lelieveld and Heintzenberg (1992). Indeed, several lines of data analysis suggest this. Most tellingly, if one examines the light-scattering efficiency of detraining air at cloud top, it significantly exceeds that of the nondetraining air in three of the five cases examined. Diagnostic modelling of the aerosol cloud processing shows that observed in cloud sulfate production, for the observed conditions, would indeed produce an enhancement in the aerosol light-scattering efficiency, though systematically lower than that observed. While none of the analyses presented are decisive in themselves, taken together they provide substantial support for cloud enhancement of the aerosol light-scattering efficiency.

5. Acknowledgments

Support for this study was provided by ONR grant N00014-97-1-0132. We wish to thank the Twin Otter pilot and co-pilot, Mike Hubbell and Roy Woods, for their skill and cooperation in flying the missions, and the staff of CIRPAS for their support. Additionally, we thank two anonymous reviewers for useful comments.

References

Anderson, T. L. and Ogren, J. A. 1998. Determining aerosol and radiative properties using the TSI 3563 integrating nephelometer. *Aerosol Sci. Technol.* **29**, 57–69.

Bates, T. S., Calhoun, J. A. and Quinn, P. K. 1992. Variations in the methanesulfonate to sulfate molar ratio in submicrometer marine aerosol particles over the Southern Pacific Ocean. *J. Geophys. Res.* **97**, 9859–9865.

Brown, E. N. and Friehe, C. A. 1983. The use of pressure fluctuations on the nose of an aircraft for measuring air motion. *J. Appl. Clim. Meteorol.* **22**, 171–180.

Buck, A. L. 1976. The variable-path Lyman-Alpha hygrometer and its operating characteristics. *Bull. Am. Meteorol. Soc.* **57**, 1113–1118.

Charlson, R. J., Schwartz, S. E., Hales, J. M., Cess, R. D., Coakley, J. A. Jr, Hansen, J. E. and Hoffmann, D. J. 1992. Climate forcing by anthropogenic aerosols. *Science* **255**, 423–430.

Friehe, C. A., Grossman, R. L. and Pann, Y. 1986. Calibration of an airborne Lyman-alpha hygrometer and measurement of water vapor flux using a thermoelectric hygrometer. *J. Atmos. Ocean. Tech.* **3**, 299–304.

Friehe, C. A. and Khelif, D. 1992. Fast-response aircraft temperature sensors. *J. Atmos. Oceanic Tech.* **9**, 784–795.

Gao, S., Hegg, D. A., Hobbs, P. V., Kirchstetter, T. W., Magi, B. J. and Sadilek, M. 2003. Water-soluble organic components in aerosols associated with savanna fires in southern Africa: identification, evolution, and distribution. *J. Geophys. Res.* **108**, SAF 27-1 to 27-16.

Hegg, D. A. 1985. The importance of liquid-phase oxidation of SO_2 in the troposphere. *J. Geophys. Res.* **90**, 3773–3779.

Hegg, D. A., Yuen, P.-F. and Larson, T. V. 1992. Modeling the effects of heterogeneous cloud chemistry on the marine particle size distribution. *J. Geophys. Res.* **97**, 12927–12933.

Heikes, B. G., Lee, M., Bradshaw, J., Sandholm, S., Davis, D. D., Crawford, J., Rodriguez, J., Liu, S., McKeen, S., Thronton, D., Bandy, A., Gregory, G., Talbot, R. and Blake, D. 1996. Hydrogen peroxide and methylhydroperoxide distributions related to ozone and odd hydrogen over the North Pacific in the fall of 1991. *J. Geophys. Res.* **101**, 1891–1905.

IPCC 2001. *Climate Change 2001, The Scientific Basis.* Cambridge University Press, Cambridge, UK.

Khelif, D., Burns, S. P. and Friehe, C. A. 1999. Improved wind measurements on research aircraft. *J. Atmos. Ocean. Tech.* **16**, 860–875.

Kogan, Y. L., Lilly, D. K., Kogan, Z. N. and Filyushkin, V. V. 1994. The effect of CCN regeneration on the evolution of stratocumulus cloud layers. *Atmos. Res.* **33**, 137–150.

Langner, J. and Rodhe, H. 1991. A global three-dimensional model of the tropospheric sulfur cycle. *J. Atmos. Chem.* **13**, 225–263.

Lelieveld, J., 1991. Multi-phase processes in the atmospheric sulfur cycle, in *NATO Advanced Workshop on C, N, P and S Biogeochemical Cycles, 4–8 March 1991, Melreux, Belgium, NATO Adv. Sci. Instrum. Ser.* (ed.R. Wollast). Kluwer Academic, Boston, MA.

Lelieveld, J. and Heintzenberg, J. 1992. Sulfate cooling effect on climate through in-cloud oxidation of anthropogenic SO_2. *Science* **258**, 117–120.

Liu, P. S. K., Leaitch, W. R., Strapp, J. W. and Wasey, M. A. 1992. Response of Particle Measurement Systems airborne ASASP and PCASP to NaCl and latex particles. *Aerosol Sci. Technol.* **16**, 83–95.

Martin, G. M., Johnson, D. W., Rogers, D. P., Jonas, P. R., Minnis, P. and Hegg, D. A. 1995. Observations of the interaction between cumulus clouds and warm stratocumulus clouds in the marine boundary layer during ASTEX. *J. Atmos. Sci.* **52**, 2902–2922.

Moenig, C.-H., 1987. Large-eddy simulation of a stratus-topped boundary layer. Part III, implications for mixed-layer modeling. *J. Atmos. Sci.* **44**, 1605–1614.

O'Sullivan, D. W., Heikes, B. G., Lee, M., Chang, W., Gregory, G., Blake, D. R. and Sachse, G. W. 1999. Distribution of hydrogen peroxide and methylhydroperoxide over the Pacific and South Atlantic oceans. *J. Geophys. Res.* **104**, 5635–5646.

Pasquill, F. 1974. *Atmospheric Diffusion*. Halsted Press, New York.

Stull, R. B. 1988. *An Introduction to Boundary Layer Meteorology.* Kluwer Academic Publishers, Boston, MA.

ten Brink, H. M., Schwarz, S. E. and Daum, P. H. 1987. Efficient scavenging of aerosol sulfate by liquid-water clouds. *Atmos. Environ.* **21**, 2035–2052.

Yuen, P.-F., Hegg, D. A. and Larson, T. V. 1994. The effects of in-cloud sulfate production on light-scattering properties of continental aerosol. *J. Appl. Meteorol.* **33**, 848–854.

Yuskiewicz, B. A., Orsini, D., Stratmann, F., Wendisch, M., Wiedensohler, A., Heintzenberg, J., Martinsson, B. G., Frank, G., Wobrock, W. and Schell, D. 1998. Changes in submicrometer particle distributions and light scattering during haze and fog events in a highly polluted environment. *Contrib. Atmos. Phys.* **71**, 33–45.

Yuskiewicz, B. A., Stratmann, F., Birmili, W., Wiedensohler, A., Swietliki, E., Berg, O. and Zhou, J. 1999. The effects of in-cloud mass production on atmospheric light scatter. *Atmos. Res.* **50**, 265–288.